

Two-dimensional and pseudo three-dimensional visualisation of foreign objects in milk carton using ultrasonic tomography

Mohd Taufiq Mohd Khairi^{a,b,*}, Sallehuddin Ibrahim^a, Mohd Amri Md Yunus^a, Mahdi Faramarzi^a

^a School of Electrical Engineering, Faculty of Engineering, Universiti Teknologi Malaysia, Skudai, Johor 81310, Malaysia

^b Forensic Engineering Group, TNB Labs Sdn Bhd, Kajang, Selangor 43000, Malaysia

ARTICLE INFO

Keywords:

Foreign bodies
Milk safety
Ultrasound
Dairy
Image reconstruction

ABSTRACT

This paper presents the development of two-dimensional and pseudo three-dimensional visualisation of foreign object in milk carton using ultrasonic tomography system. Mathematical modelling based on ultrasonic amplitude wave and correlation between ultrasonic projection distance and voltage sensor are elaborated in this paper. Physical hazard contaminants such as metal, plastic, wood and glass materials were placed in the milk. The forward problem and the inverse problem of image reconstruction technique have been discussed briefly. 2D images of the contaminants are reconstructed using Linear Back-Projection (LBP) and Convolution Back-Projection (CBP) with Hanning, Hamming and Ram-Lak filter. A median filter technique has been combined to the algorithms for filtering noise of reconstructed images. The results show that image reconstruction using CBP-Ram-Lak has significantly yield the best image reconstruction for most tested phantoms. The application of median filter with 20×20 matrix have obtained a better image quality as they achieved the best values of PSNR and SSIM compared to non-median filter with 13.2765 and 0.7318, respectively for pairs of metal A - glass B (phantom Y-2). Pseudo three-dimensional (3D) image reconstruction for the foreign object has been carried out to provide more sufficient monitoring process in milk cartons. The 3D images were constructed based on stacking the 2D slice images in z -axis. Thus, the exact location of the object in the milk carton can be exposed clearly from various viewing angles. The results indicate that the ultrasonic tomography imaging system promises to be a non-invasive tool in quality monitoring especially for the detection of foreign objects in milk carton.

1. Introduction

In dairy industry, safety and quality of products are emphasized by manufacturers. Dairy product contamination must be avoided because it has a negative impact on a large scale. Dairy product can be contaminated by three hazardous categories i.e.; biological, chemical and physical hazards. Park et al [1]. analysed food incidents due to chemical, biological and physical hazards in South Korea that occurred between January 1998 and March 2016. 975 cases were recorded during this period where 199 cases were due to physical hazard and 9 cases involved dairy product. Djekic et al [2]. analysed the presence of foreign objects from 1998 to 2015 in 31 European countries. During this period, 43 out of 1446 cases were found to occur in dairy products. In Brazil, a study of foreign objects in food from 2001 to 2015 was performed by Mattos et al [3]. The results revealed that 57 out of 719 cases of foreign objects were found in dairy products. A detailed study of foreign objects existence in dairy product was performed by Aguiar et al [4]. where the scope of the research covers Brazil from year 2012 to 2016. The results show that 515 complaints were reported with yogurt/milk

drink showing the highest percentage of the foreign objects existence with 37%, followed by ultra-high temperature (UHT) milk (14.6%) and milk powder (10.7%). There are also several cases involving the presence of objects in milk drink had been reported by the press as listed in Table 1. The reported cases have created a concern among the consumers, therefore it is vital for manufacturers to use a variety of tools and sensors as a proactive measure to ensure that their products are free from the presence of foreign objects.

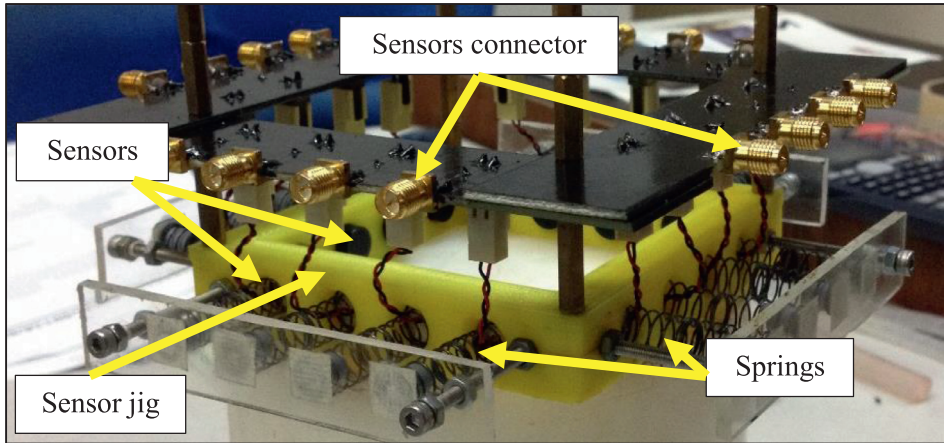
There are several non-invasive methods that have been used to detect foreign objects. Non-invasive techniques are attractive as they can be used to detect the foreign objects without affecting the ingredient and the original form of the food. The methods comprise of X-ray, thermal imaging, hyperspectral imaging and terahertz. However, these methods have their own weaknesses and have restricted their applications. For example, X-ray has several disadvantages in terms of economical aspect which is high cost and high power usage [15,16]. Thermal imaging technique needs to overcome temperature interference from other surfaces [17]. Hyperspectral imaging requires a lengthy time for pre-processing of the data and classification [18,19]. Whereas, terahertz

* Corresponding author.

E-mail addresses: taufiq_khairi@yahoo.com (M.T.M. Khairi), salleh@fke.utm.my (S. Ibrahim).

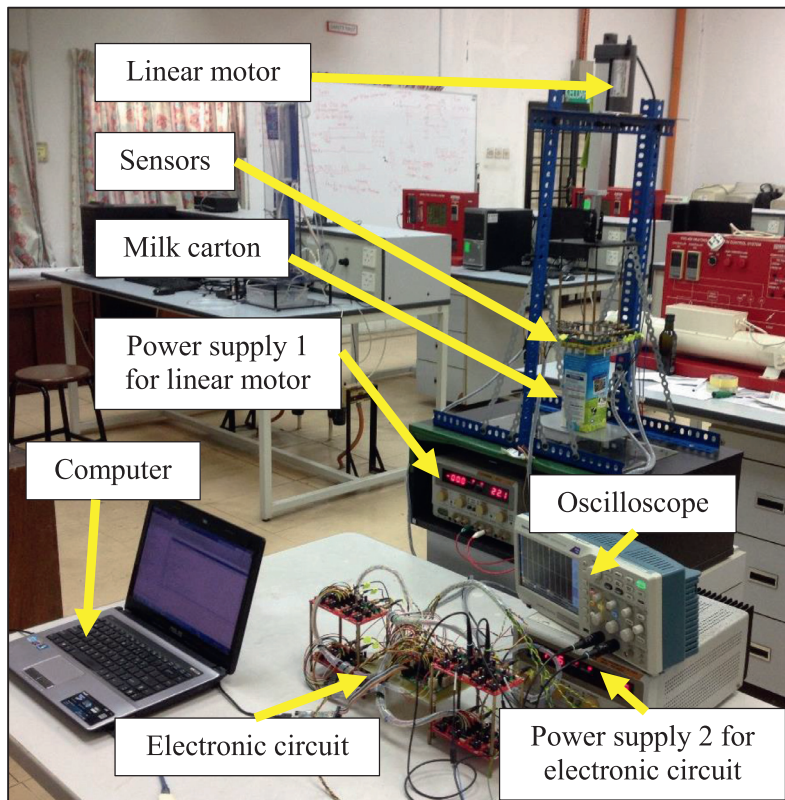
Table 1
Cases of physical contamination in dairy milk.

| Contamination | Date | Reference |
|---------------------|------------|---|
| Unidentified object | 23/6/2009 | BBC News 2009 [5] |
| Glass | 7/4/2011 | CBC News 2011 [6] |
| Needle | 29/9/2011 | BBC News 2011 [7] |
| Hair | 19/4/2012 | Australia Food News 2012 [8] |
| Mould | 1/4/2015 | CBC News 2015 [9] |
| Screw | 5/6/2015 | KomoneWS 2015 [10] |
| Plastic | 19/7/2015 | Sfgate 2015 [11] |
| Unidentified object | 26/3/2016 | Hong Kong Free Press 2016 [12] |
| Unidentified object | 26/10/2016 | Channel News Asia 2016 [13] |
| Metal | 27/7/2018 | Food Standard Australia New Zealand 2018 [14] |



(a)

Fig. 1. (a) The setup of the sensors, the sensor jig and the springs (b) The complete measurement system.



(b)

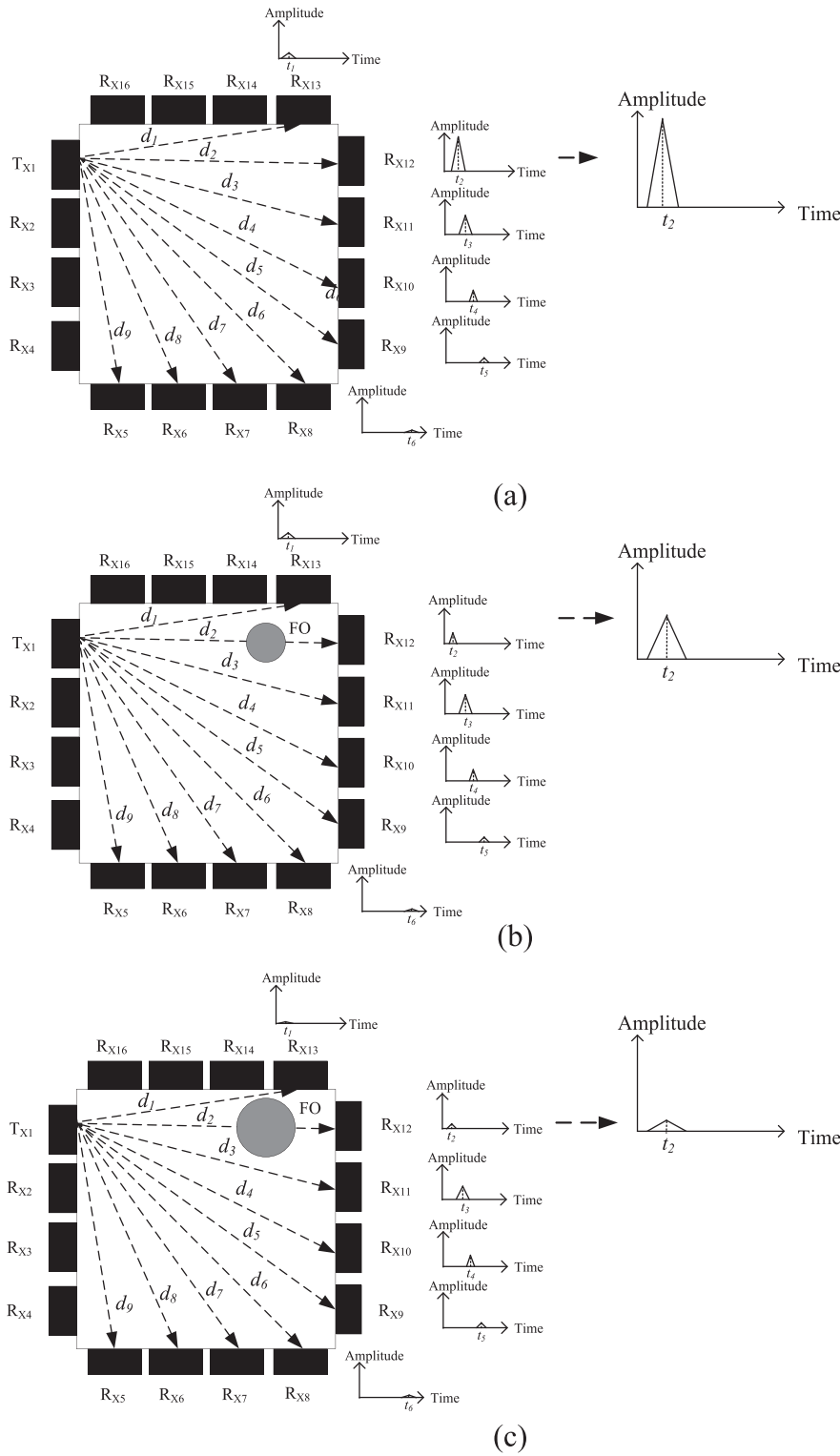


Fig. 2. Ultrasonic sensors for amplitude analysis using the transmission sensing mode for T_{x1} (a) No foreign object in the milk carton (b) A small foreign object in the milk carton (c) A large foreign object in the milk carton.

waves has weakness to penetrate in water medium since the signal is highly attenuated in such medium [16].

Ultrasound is a non-invasive technique that attracts interest in the food industry as it low cost, easy to be automated online and is safe from radiation [20]. The ultrasonic technique merged with an imaging technique called tomography could improve the effectiveness in detecting foreign objects in milk cartons. Ultrasonic tomography is a technique that consists of several sensors which are located externally to the test

material surface and it can unravel the inside condition without disturbing the original condition of the material [21,22]. A tomographic image is reconstructed based on the following steps. First, the formation of sensitivity maps. Next, the property field is reconstructed based on the measured integral values using an image reconstruction algorithm [23].

In dairy industry, the colour of the milk produced by the manufacturer is produced in a variety of flavours such as strawberry, chocolate, fresh milk and full cream. Hence, the milk colour is not transparent.

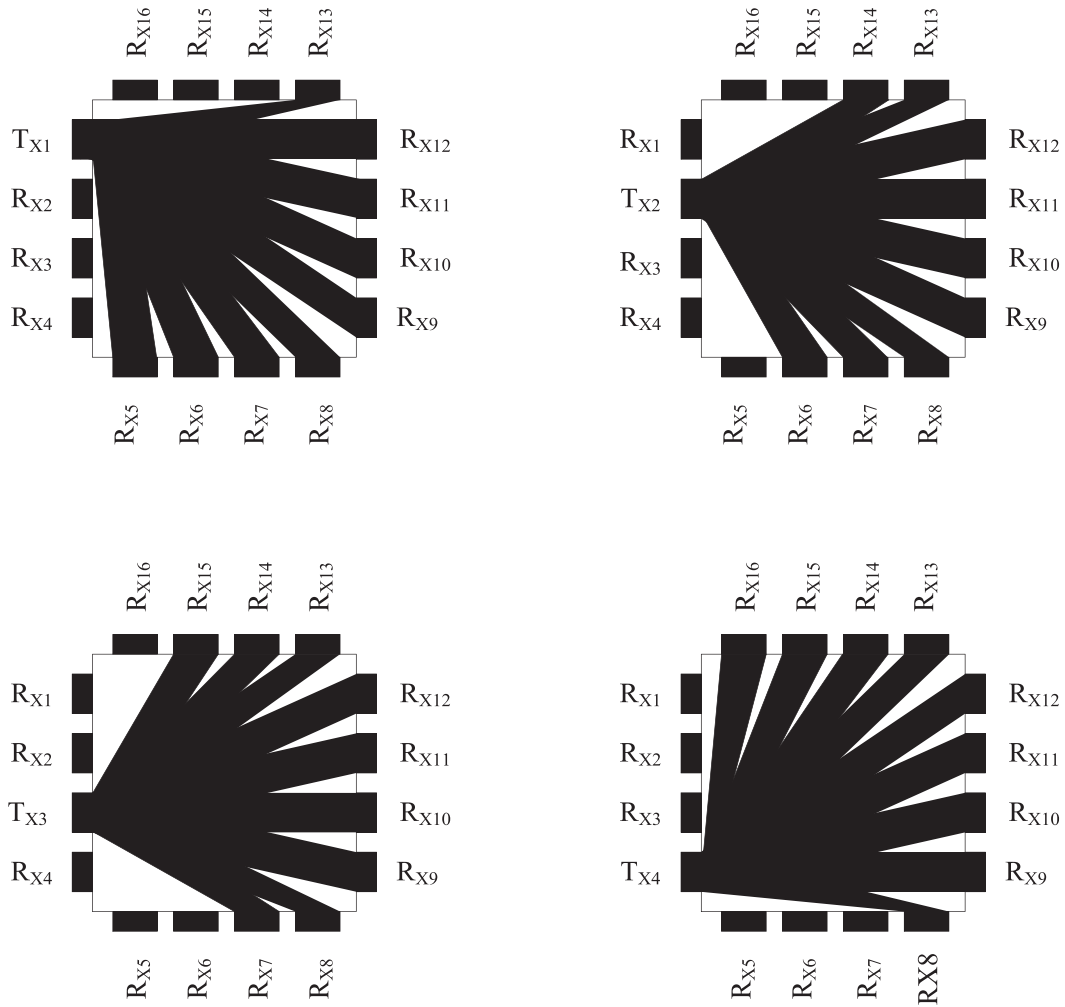


Fig. 3. The projection path for transmitters TX1, TX2, TX3 and TX4. 3. (a) The setup of the sensors, the sensor jig and the springs (b) The complete measurement system.

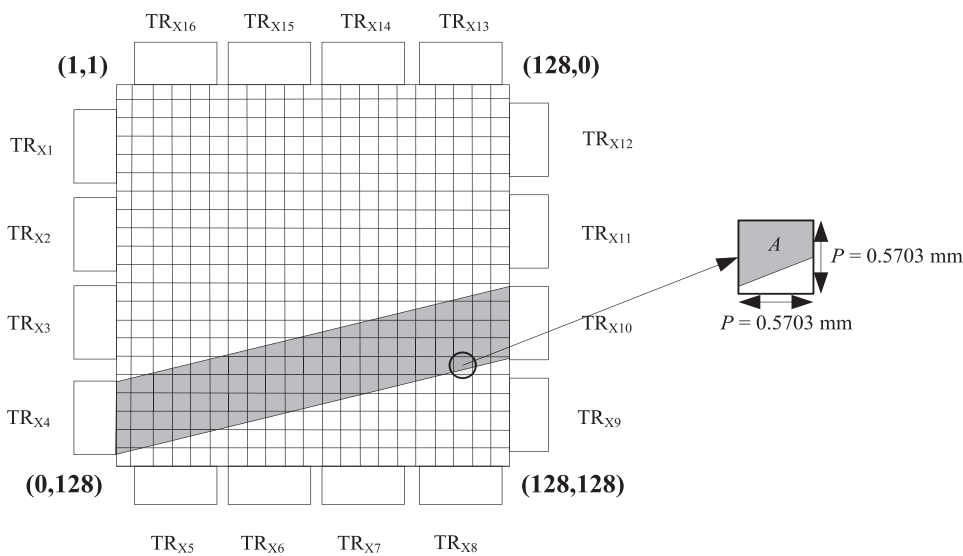


Fig. 4. Projection path from sensor TR_{x4} to receiving sensor TR_{x10}.

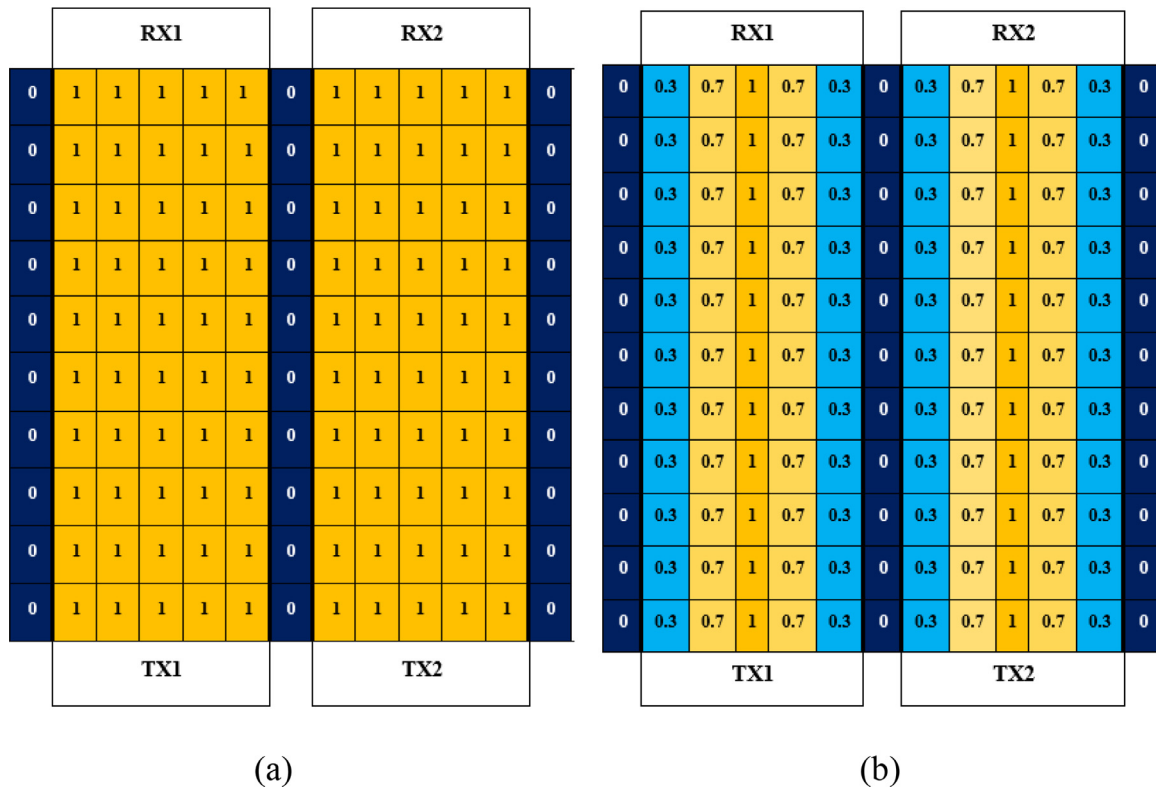


Fig. 5. Sensitivity map for $T_{X1} - R_{X1}$ and $T_{X2} - R_{X2}$ (a) Linear sensitivity map (b) Exponential sensitivity map.

Table 2
Receivers' voltages when transmitter T_{X1} is on.

| Receiver (R_x) | Distance, d (mm) | Measured voltage (V) |
|--------------------|--------------------|----------------------|
| R_{X5} | 62 | 0.08 |
| R_{X6} | 67 | 0.42 |
| R_{X7} | 75 | 0.13 |
| R_{X8} | 87 | 1.15 |
| R_{X9} | 88 | 2.17 |
| R_{X10} | 80 | 3.49 |
| R_{X11} | 75 | 3.42 |
| R_{X12} | 73 | 4.64 |
| R_{X13} | 63 | 0.01 |

Table 3
Receivers' voltages when transmitter T_{X2} is on.

| Receiver (R_x) | Distance, d (mm) | Measured voltage (V) |
|--------------------|--------------------|----------------------|
| R_{X6} | 51 | 0.35 |
| R_{X7} | 61 | 0.24 |
| R_{X8} | 75 | 0.45 |
| R_{X9} | 80 | 2.14 |
| R_{X10} | 74 | 3.42 |
| R_{X11} | 73 | 4.84 |
| R_{X12} | 74 | 4.59 |
| R_{X13} | 69 | 0.05 |
| R_{X14} | 53 | 0.35 |

Table 4
Receivers' voltages when transmitter T_{X3} is on.

| Receiver (R_x) | Distance, d (mm) | Measured voltage (V) |
|--------------------|--------------------|----------------------|
| R_{X7} | 53 | 0.66 |
| R_{X8} | 67 | 0.09 |
| R_{X9} | 74 | 3.24 |
| R_{X10} | 73 | 4.48 |
| R_{X11} | 74 | 3.22 |
| R_{X12} | 80 | 2.77 |
| R_{X13} | 76 | 0.07 |
| R_{X14} | 64 | 0.53 |
| R_{X15} | 54 | 1.12 |

Table 5
Receivers' voltages when transmitter T_{X4} is on.

| Receiver (RX) | Distance, d (mm) | Measured voltage (V) |
|---------------|--------------------|----------------------|
| R_{X8} | 63 | 0.02 |
| R_{X9} | 73 | 4.22 |
| R_{X10} | 75 | 3.98 |
| R_{X11} | 80 | 2.27 |
| R_{X12} | 88 | 2.21 |
| R_{X13} | 87 | 0.05 |
| R_{X14} | 75 | 0.51 |
| R_{X15} | 67 | 0.55 |
| R_{X16} | 62 | 0.02 |

Therefore, it is quite difficult to see if there are foreign object in the box/bottle unless knocking sound is heard while pouring milk into the cup [20]. Otherwise, the object could be noticeable if it is floating on the surface of the cup. The foreign object has the potential to harm the consumer if swallowed accidentally.

Early detection of foreign objects is an important control measure in ensuring the safety and quality of dairy product. The company will conduct a detailed investigation to find out what type of foreign object is, where can it came from and the types of dangers that may arise from

a safety perspective [24,25]. This procedure is to prevent the same incident from recurring and makes numerous efforts to avoid unwanted foreign objects in their products. Non-invasive technique has become a choice to perform an early assessment since the original form of the dairy product are not affected during the evaluation process.

This paper proposes an ultrasonic tomography system, as a non-destructive method to detect and visualise the foreign objects in a milk carton based on the two-dimensional (2D) and pseudo three-

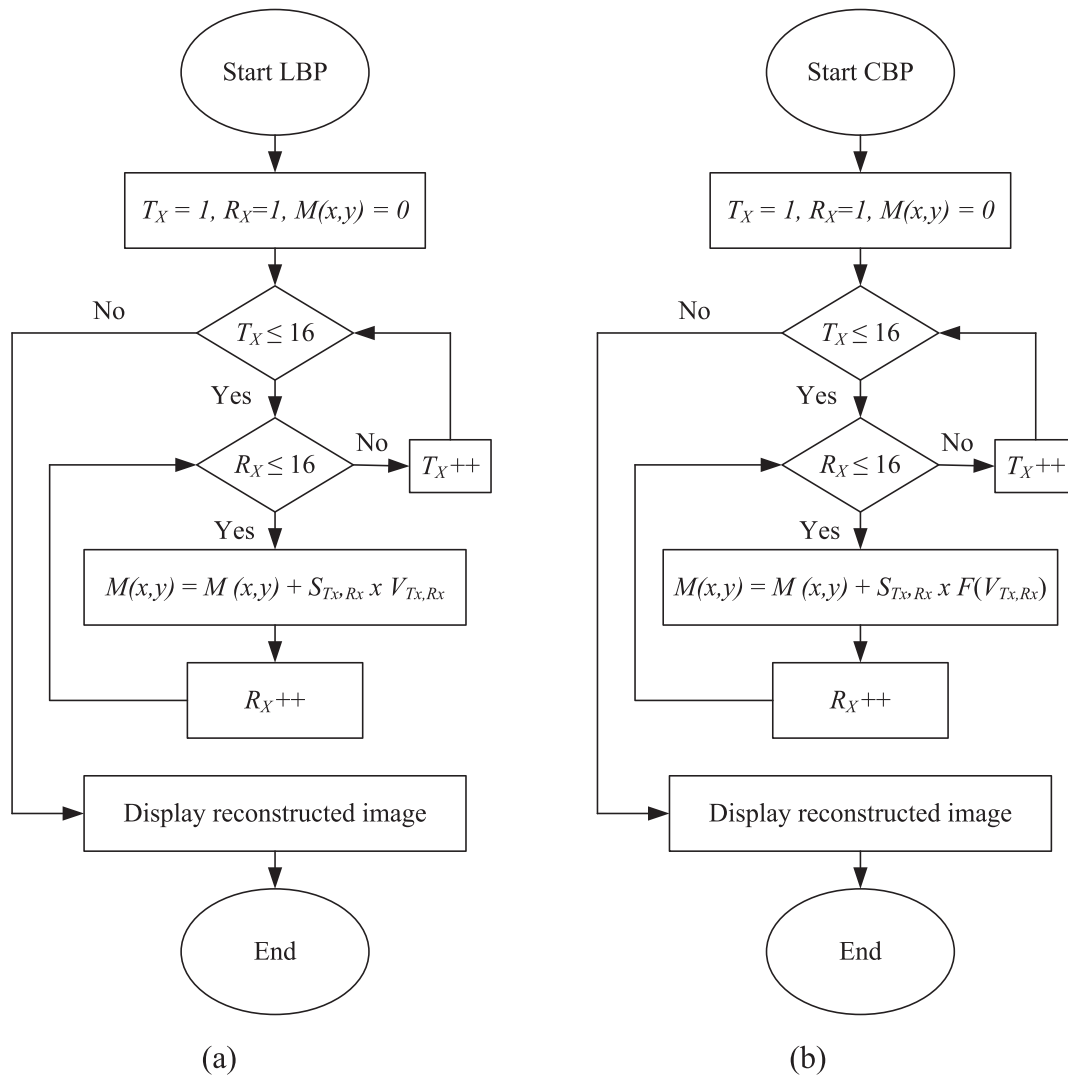


Fig. 6. Flowcharts (a)LBP algorithm (b) CBP algorithm.

| | | |
|----|-----|----|
| 18 | 22 | 33 |
| 34 | 128 | 24 |
| 22 | 19 | 32 |

(a)

| | | |
|----|----|----|
| 18 | 22 | 33 |
| 34 | 24 | 24 |
| 22 | 19 | 32 |

(b)

Fig. 7. An example of a median filter (a) input of 3 × 3 pixels (b) output of 3 × 3 pixels.

dimensional (3D) reconstructed image. Hence, the indication and location of foreign objects can be observed. Therefore, the ultimate research question is how to provide both design specification and description of an ultrasonic tomography system for detecting the foreign objects in milk carton. This research is an extension work from previous article [20] where this paper focuses on the ultrasonic modelling based on amplitude wave and projection sensors. This paper also used irregular size of materials compared to previous article which has used specific size of rod as test samples. The image reconstruction comprises of forward

problem, inverse problem, median filter, 2D and pseudo 3D image reconstruction also discussed in this paper.

2. Materials and methods

2.1. Ultrasonic tomography system

The experiment was conducted using pasteurised chocolate milk manufactured by the Dutch Lady company. The system consists of a square shaped sensor jig, an electronic circuit, a linear motor and a display system. The sensor jig has a dimension of 96 mm × 96 mm and has sixteen holes for sensor placement. A spring is used to push the sensor to ensure that the sensors are always in contact with the milk carton. The setup of spring and the complete setup of an ultrasonic tomography measurement system is shown in Fig. 1 (a) and Fig. 1 (b), respectively. Sixteen ultrasonic transceivers with a frequency of 333 kHz are placed outside a milk carton which has a cross-sectional dimension of 73 mm × 73 mm. Coaxial cable is used to connect the sensors and the electronic circuit. The cable ensures that the noise between the connection can be minimized. The linear motor has a speed of 20 mm/s, 24 V rated voltage direct current and is driven using the MD10C motor driver module. The module is designed to drive high current brushed DC motor up to 13A continuously.

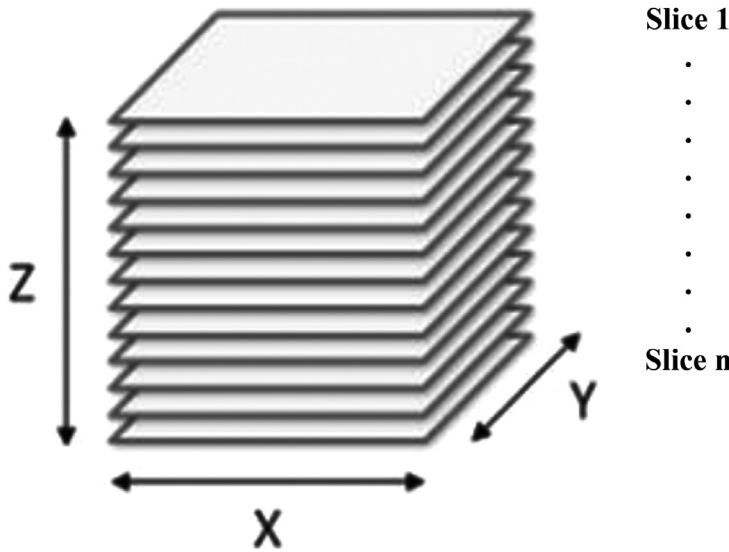


Fig. 8. The stacking process of 2D slices images.

Table 6
Linear and exponential sensitivity map for some example of projection paths.

| Projection path | Linear sensitivity map | Exponential sensitivity map | Colour bar |
|-----------------------|------------------------|-----------------------------|------------|
| T_{X5} to R_{X13} | | | |
| T_{X5} to R_{X15} | | | |
| T_{X5} to R_{X15} | | | |
| T_{X5} to R_{X16} | | | |

A 16-bit microcontroller unit model dsPIC30F6014A manufactured by Microchip was used to perform six main tasks; control the linear motor, switching selection, generates transmitter signal, generates sample/hold signal, converts analogue value to digital value and transfer the data to the computer. A PIC C Compiler software was used to write and compile the programming code to the microcontroller. Two digital outputs from microcontroller ports are connected to the pulse width modulation (PWM) and directional (DIR) pin in motor driver module MD10C to control the linear motor. The other tasks used 16 ports, hence 64 ports are required from the microcontroller unit. The microcontroller unit has a total of 68 bidirectional input/output. 16 analogue input channels ports (AN0 to AN15) are used for analogue-to-digital conversion (ADC) purpose. These channels have 12-bit with 200 kg samples per second (Ksps) conversion rate.

Table 7
Types of foreign objects.

| Material types | Foreign objects | Length (l) |
|----------------|-----------------|----------------------------|
| Wood | | A: 21.38 mm B: 13.23 mm |
| Glass | | A: 15.69 mm B: 13.17 mm |
| Metal | | A: 19.36 mm B: 13.06 mm |
| Plastic | | A: 20.66 mm B: 12.32 mm |

2.2. Mathematical modelling of ultrasonic – amplitude wave

The analysis of the amplitude wave is one of approach to determine whether the milk contains any foreign object or not. The transmitted wave has a certain wave energy level that can be detected by a receiver. However, the energy amplitude level dropped when it reached the receiver due to several factors. The first factor is that the wave energy attenuates when it travels through the milk. The attenuation is based on

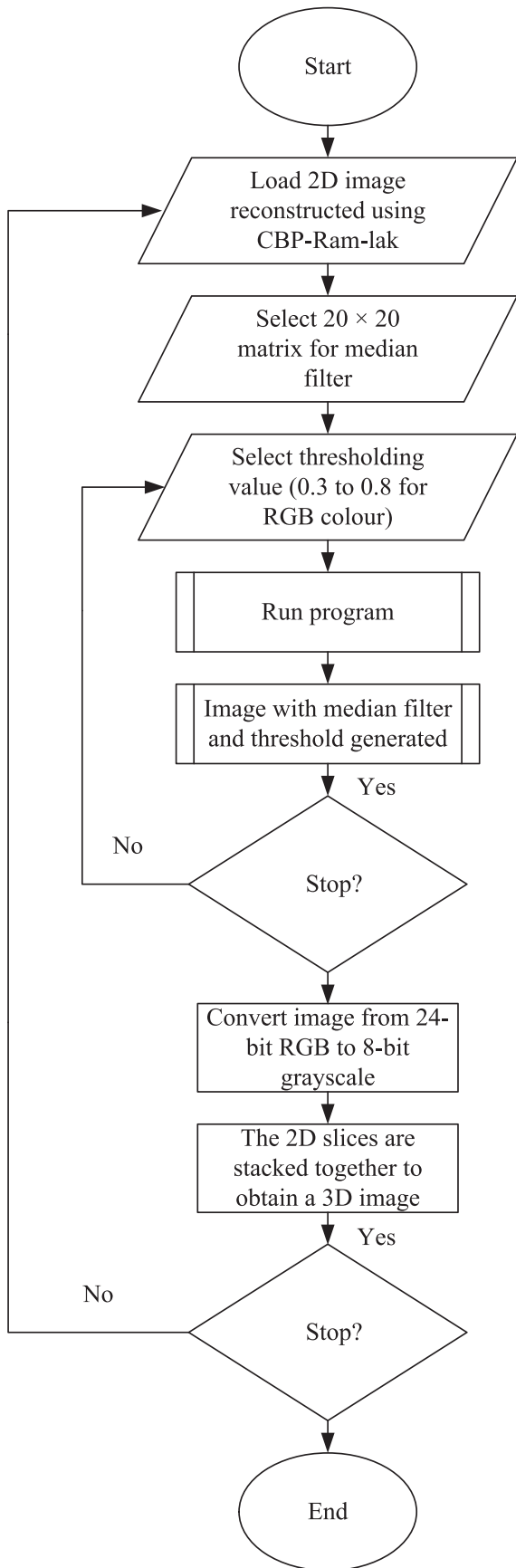


Fig. 9. Pseudo 3D image reconstruction steps from 2D slice images.

Table 8
Reconstructed images without median filter.

| Phantom | LBP | CBP-Hamm | CBP-Hann | CBP-Ram-lak |
|---------------------------|-----|----------|----------|-------------|
| Metal A-Metal B (X-1) | | | | |
| Metal A-Glass B (X-2) | | | | |
| Metal A-Plastic B (X-3) | | | | |
| Metal A-Wood B (X-4) | | | | |
| Plastic A-Plastic B (X-5) | | | | |
| Plastic A-Metal B (X-6) | | | | |
| Plastic A-Glass B (X-7) | | | | |
| Plastic A-Wood B (X-8) | | | | |
| Glass A-Glass B (X-9) | | | | |
| Glass A-Metal B (X-10) | | | | |

(continued on next page)

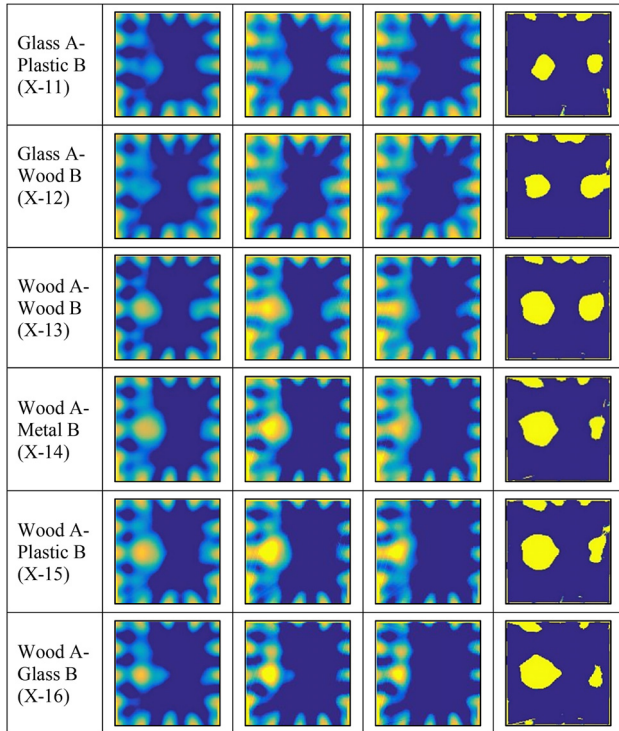
the Beer-Lambert law which can be written as:

$$A_R = A_T e^{-\alpha L} \tag{1}$$

where A_R and A_T are the receiver amplitude and the transmitter amplitude respectively, L is the length of the milk carton and α is the combined attenuation coefficients for milk and milk carton. The equation shows that the wave amplitude exponentially decreased with respect to the attenuation coefficients of milk and the length of the milk cartons (the distance between the transmitters and receivers) as shown in Fig. 2(a). The amplitude levels sensed by receivers R_{X5} , R_{X6} , R_{X7} , R_{X8} , R_{X9} , R_{X10} and R_{X11} seem to be lower than the amplitude sensed by R_{X12} and R_{X13} since they have longer distances with T_{X1} .

The amplitude also can be reduced if a foreign object disturbed the propagation path of the wave. The size of the foreign object also influenced the amplitude level. The larger size of the foreign object led to more reduction in the amplitude due to the wave being blocked from

Table 8 (continued)



propagating to the receiver. In Fig. 2(a), R_{X12} senses the highest amplitude since the distance between the R_{X12} and T_{X1} has the shortest distance and does not contain any foreign object. However, the amplitude level is reduced when a foreign object exists along the wave propagation path as illustrated in Fig. 2(b) and (c).

2.3. Mathematical modelling of ultrasonic – projection distance and voltage sensor

The transmission mode and fan beam projection are proposed in this research. The sensor type is transceiver where each sensor can function either as a transmitter or as a receiver. When one transceiver is operated as transmitter, the remaining fifteen sensors would be operated

as receivers. However, not all receivers can sense the wave projected from the transmitter since the angle of beam for this sensor is not too wide which is around 10° . As can be seen in Fig. 3, only nine receivers have detected the transmitted wave when transmitters T_{X1} to T_{X4} emit ultrasonic waves. An experiment has been performed to investigate the correlation between the voltage and the receivers’ position when a transmitter is operated. The results for transmitters T_{X1} to T_{X4} are tabulated in Tables 2 to 5. The voltage has the highest value when the transmitter and the receiver are located in front of each other. The voltages decrease when the receivers are further away from the transmitter. For transmitter T_{X1} , receiver R_{X12} has the highest value with 4.64 V, followed by R_{X10} (3.49 V) and R_{X11} (3.42 V). For transmitter T_{X2} , receiver R_{X11} has the highest value with 4.84 V, followed by R_{X12} (4.59 V) and R_{X10} (3.42 V). For transmitter T_{X3} , receiver R_{X10} has the highest value with 4.48 V, followed by R_{X11} (3.24 V) and R_{X9} (3.22 V). For transmitter T_{X4} , receiver R_{X9} has the highest value with 4.22 V, followed by R_{X10} (3.98 V) and R_{X11} (2.27 V).

The data also indicated that when the axis of the receiver is perpendicular to the transmitter wave, the receiver has a small voltage value although it is close to the transmitter. On the other hand, the receivers which have axes that are not within the sensor beam angle are still able to detect the wave. This may be due to the refraction that occurs between wave and milk. If the foreign object located at outer of the testing domain, the sensor could not able to detect it existence. The voltages measured for the remaining transmitters T_{X5} - T_{X16} are almost similar with transmitters T_{X1} - T_{X4} .

2.4. Image reconstruction algorithm

2.4.1. Forward problem

Image reconstruction for tomography measurement system comprises of forward problem and inverse problem. The forward problem deals with the approximation of the sensor readings by modelling the sensor projection. Whereas, the inverse problem deals with the reconstruction image using the sensor reading using the image reconstruction algorithm. The algorithm that has been used is Linear back-projection (LBP) and Convolution back-projection (CBP) with Hamming, Hanning and Ram-Lak filters. The forward problem is initially performed by discretizing the region of interest (ROI) into 128×128 pixels for all sixteen ultrasonic sensors projections. The ROI for this ultrasonic tomography system is a milk carton which has a square shape and a dimension of $73 \text{ mm} \times 73 \text{ mm}$. Each small pixel in the ROI can be determined accord-

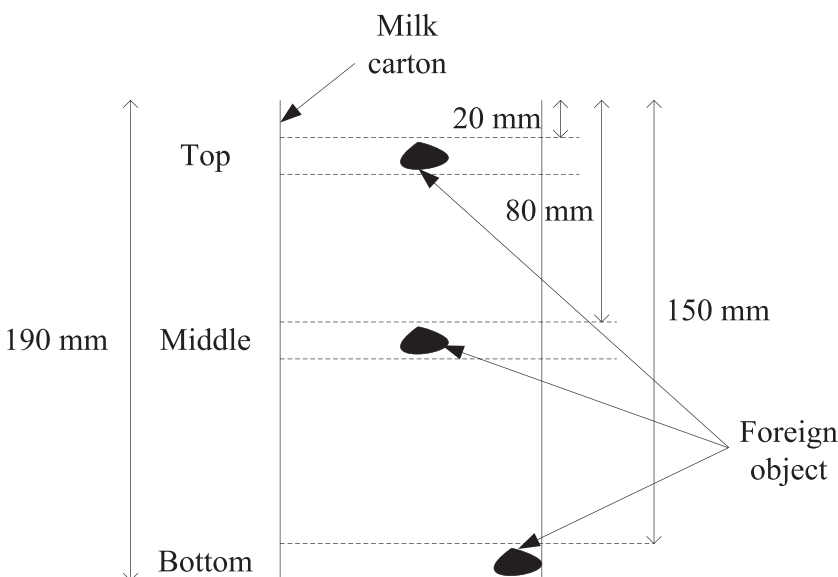


Fig. 10. The location of the foreign object that had being be tested.

Table 9
Reconstructed images with a median filter application.

| Phantom | LBP Mfilter | CBP-Hamm Mfilter | CBP-Hann Mfilter | CBP-Ram-lak Mfilter |
|---------------------------|-------------|------------------|------------------|---------------------|
| Metal A-Metal B (Y-1) | | | | |
| Metal A-Glass B (Y-2) | | | | |
| Metal A-Plastic B (Y-3) | | | | |
| Metal A-Wood B (Y-4) | | | | |
| Plastic A-Plastic B (Y-5) | | | | |
| Plastic A-Metal B (Y-6) | | | | |
| Plastic A-Glass B (Y-7) | | | | |
| Plastic A-Wood B (Y-8) | | | | |
| Glass A-Glass B (Y-9) | | | | |
| Glass A-Metal B (Y-10) | | | | |
| Glass A-Plastic B (Y-11) | | | | |
| Glass A-Wood B (Y-12) | | | | |
| Wood A-Wood B (Y-13) | | | | |

(continued on next page)

Table 9 (continued)

| | | | | |
|-------------------------|--|--|--|--|
| Wood A-Metal B (Y-14) | | | | |
| Wood A-Plastic B (Y-15) | | | | |
| Wood A-Glass B (Y-16) | | | | |

ing to the following equation:

$$P = \frac{S}{N} = \frac{73 \text{ mm}}{128 \text{ pixels}} = 0.5703 \text{ mm} \quad (2)$$

where P is the pixel size, S is the carton size and N is the number of pixels in the ROI. The square shape carton with 73 mm of length is discretized into an image plane which has a total pixel of 16,384.

Since the transmission-mode of projection is utilised, hence it is assumed that the projection from the transmitter sensor to receiver sensor is in a straight-line path as illustrated in Fig. 4. The sensitivity map in each pixel array for sensor projection (x, y) position can be obtained from the following equation.

$$S_{T_x, R_x}(x, y) = \frac{A}{P^2} \quad (3)$$

where $S_{T_x, R_x}(x, y)$ is the sensitivity at position (x, y) from transmitter T_x to receiver R_x , A is the area of pixel occupied by a projection and P is the pixel size.

Two types of sensitivity maps which are linear [26,27] and exponential [28,29] are investigated and discussed. A linear sensitivity map is commonly used since it is a simple method in creating the sensitivity map for the projection path of the sensors. Values of 0 and 1 are fixed to non-active and active projection path, respectively as shown in Fig. 5(a). A non-active projection path means the wave does not traverse through the path. On the other hand, an active path means the pixels are occupied and located inside the projection path. A linear sensitivity map has a drawback in that it can produce a blurry image. Thus, an exponential sensitivity map is utilized to reduce these problems.

This type of sensitivity map had been successfully applied by for visualizing two and three phase flow regimes using a tomography system. It is based on the exponential of distance from the middle of the path as shown in Fig. 5(b) where the value exponentially decreases from 1 until 0.3. The sensitivity map can be formulated as:

$$S_{T_x, R_x}(x, y) = e^{-(x^2+y^2)/\sigma} \quad (4)$$

where $S_{T_x, R_x}(x, y)$ is the sensitivity map from transmitter T_x to receiver R_x , σ is the standard deviation of the Gaussian distribution, x and y are the pixel centre point coordinate Table 6. shows the comparison between linear and exponential sensitivity maps for sensors $T_{X5} - R_{X13}$, $T_{X5} - R_{X14}$, $T_{X5} - R_{X15}$ and $T_{X5} - R_{X16}$. The projection path is filled with values of 1 for the linear projection path, whereas the value exponentially decreased from 1 to 0.3 for the exponential sensitivity map.

2.4.2. Inverse problem

There are numerous solutions to solve the inverse problem in order to reconstruct an image from the sensor readings. Two types of algorithms that are commonly used in the computed tomography technique are analytical and iterative algorithms. Examples of an analytical algorithm are linear back-projection (LBP) and convolution back-projection (CBP) [30]. Examples of an iterative algorithm are algebraic

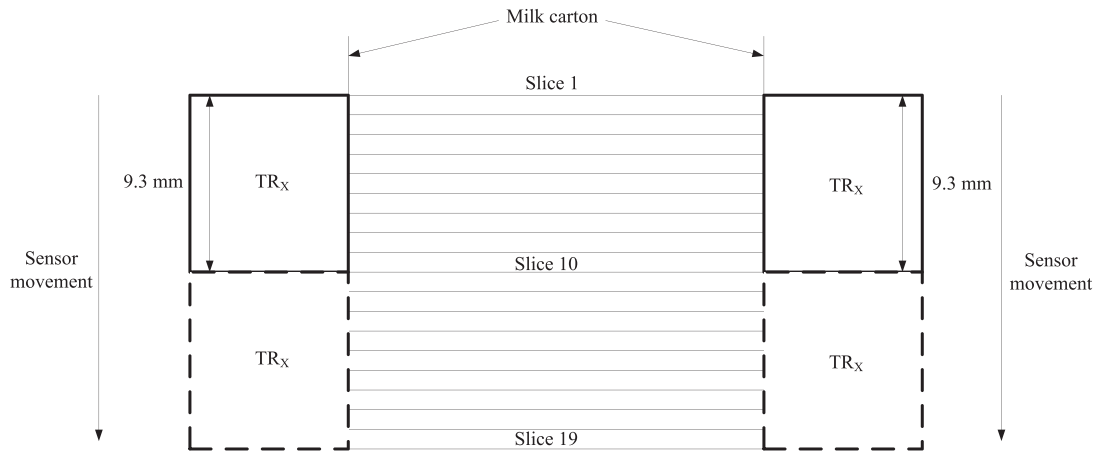


Fig. 11. The illustration of the size of sensors and the image slices.

Table 10
PSNR and SSIM index for group without median filter.

| Phantom | LBP | | CBP-Hamm | | CBP-Hann | | CBP-Ram-Lak | |
|---------|----------------|--------|-----------|--------|-----------|---------------|----------------|---------------|
| | PSNR (dB) | SSIM | PSNR (dB) | SSIM | PSNR (dB) | SSIM | PSNR (dB) | SSIM |
| X-1 | 9.8739 | 0.4076 | 9.6290 | 0.3769 | 9.3274 | 0.3082 | 11.2916 | 0.6274 |
| X-2 | 10.1935 | 0.4743 | 9.6786 | 0.3661 | 9.3580 | 0.3104 | 13.2687 | 0.7234 |
| X-3 | 10.3337 | 0.4999 | 9.9169 | 0.4229 | 9.8221 | 0.3800 | 12.4758 | 0.7017 |
| X-4 | 10.5301 | 0.4959 | 10.1152 | 0.4384 | 10.0602 | 0.4140 | 12.4194 | 0.6738 |
| X-5 | 10.7604 | 0.5296 | 10.1195 | 0.4603 | 9.8827 | 0.4189 | 11.4931 | 0.6525 |
| X-6 | 10.9046 | 0.5423 | 9.4386 | 0.3387 | 9.1125 | 0.2710 | 10.1402 | 0.5498 |
| X-7 | 10.4047 | 0.4958 | 10.0198 | 0.4119 | 9.6482 | 0.3449 | 11.3525 | 0.6321 |
| X-8 | 10.5495 | 0.5061 | 9.6516 | 0.3641 | 9.5053 | 0.3155 | 11.2429 | 0.6344 |
| X-9 | 10.3227 | 0.4878 | 9.8474 | 0.3902 | 9.6563 | 0.3446 | 12.0135 | 0.6594 |
| X-10 | 10.2856 | 0.4794 | 9.3261 | 0.3124 | 8.9936 | 0.2563 | 12.0716 | 0.6749 |
| X-11 | 10.2857 | 0.4915 | 9.9153 | 0.4477 | 9.8892 | 0.4256 | 12.1496 | 0.6752 |
| X-12 | 10.1411 | 0.4261 | 9.4943 | 0.3547 | 9.2408 | 0.2860 | 11.5711 | 0.6461 |
| X-13 | 10.0092 | 0.4160 | 9.9836 | 0.4228 | 9.5409 | 0.3423 | 10.7361 | 0.5954 |
| X-14 | 10.2936 | 0.4434 | 10.2889 | 0.4419 | 9.7934 | 0.3662 | 11.3184 | 0.6287 |
| X-15 | 10.9812 | 0.5301 | 10.9240 | 0.5407 | 10.5662 | 0.5039 | 11.4672 | 0.6418 |
| X-16 | 10.1523 | 0.4507 | 10.4197 | 0.4831 | 10.1889 | 0.4437 | 11.7196 | 0.6500 |
| Average | 10.3764 | 0.4798 | 9.9230 | 0.4108 | 9.6616 | 0.3582 | 11.6707 | 0.6479 |
| SD | 0.3056 | 0.0409 | 0.4059 | 0.0587 | 0.4137 | 0.0687 | 0.7359 | 0.0404 |

*Bold numbers show the highest value of the test phantom.

reconstruction technique (ART), simultaneous algebraic reconstruction technique (SART) and simultaneous iterative reconstruction technique (SIRT) [31]. In terms of image reconstruction processing time, the analytical algorithm has a better performance compared to the iterative algorithm [32]. However, the iterative method is better than the analytical method in terms of noise reduction and improving quantitative accuracy [33]. This paper discusses the analytical algorithms which are LBP and CBP. The flowcharts for the LBP and CBP algorithms are shown in Fig. 6. The program starts with initializing transmitter (T_x), receiver (R_x) and image matrix ($M(x,y)$) to 1, 1 and 0, respectively. Then, each loop one projection is multiplied by the sensitivity map ($S_{TX, RX}$). The resulted matrix is added to the $M(x,y)$ using the LBP and CBP equation. Finally, the image is reconstructed and displayed in the computer.

2.5. Median filter

Image filters for reducing noise can be categorized into two types; linear and non-linear. A convolution filter is an example of a linear filter where it encompassed a matrix multiplication. A median filter is a non-linear type where it operated by moving through the image pixel by pixel and replacing each value with the median value of neighbouring pixels [34]. It is effectively used in image processing to reduce 'salt and pepper' type noise inside an $m \times n$ window [18]. It works by rearranging all the pixel value into an ascending order, then replacing the pixel being

considered with the middle (median) pixel value. An example on how the median filter works is discussed below. Let say there is 3×3 pixels of image as shown in Fig. 7. The value of 128 indicates the presence of noise since it shows the uncommon value.

The steps for the median filter are:

1. The values are rearranged in ascending order.
18, 19, 22, 22, 24, 32, 33, 34, 128
2. The median number of the order is 24.
3. The value of 24 replaced the value of 128 in the middle pixel as shown in Fig. 7(b).
4. The process is continued for the next pixel if there is a larger size of window.

2.6. Image quality assessment

The reconstructed images using an ultrasonic tomography system has utilised two computerised image assessments; the peak signal-to-noise ratio (PSNR) and structural similarity (SSIM). The other qualitative methods that widely used are Visible Differences Predictor (VDP) and Anisotropy (LMQ). VDP has limitation where it does not work with colour information and it only work with brightness. Whereas, LMQ not has a fair correlation when images are noisy [35]. PSNR is a simple method for image quality assessment. PSNR can be easily defined by

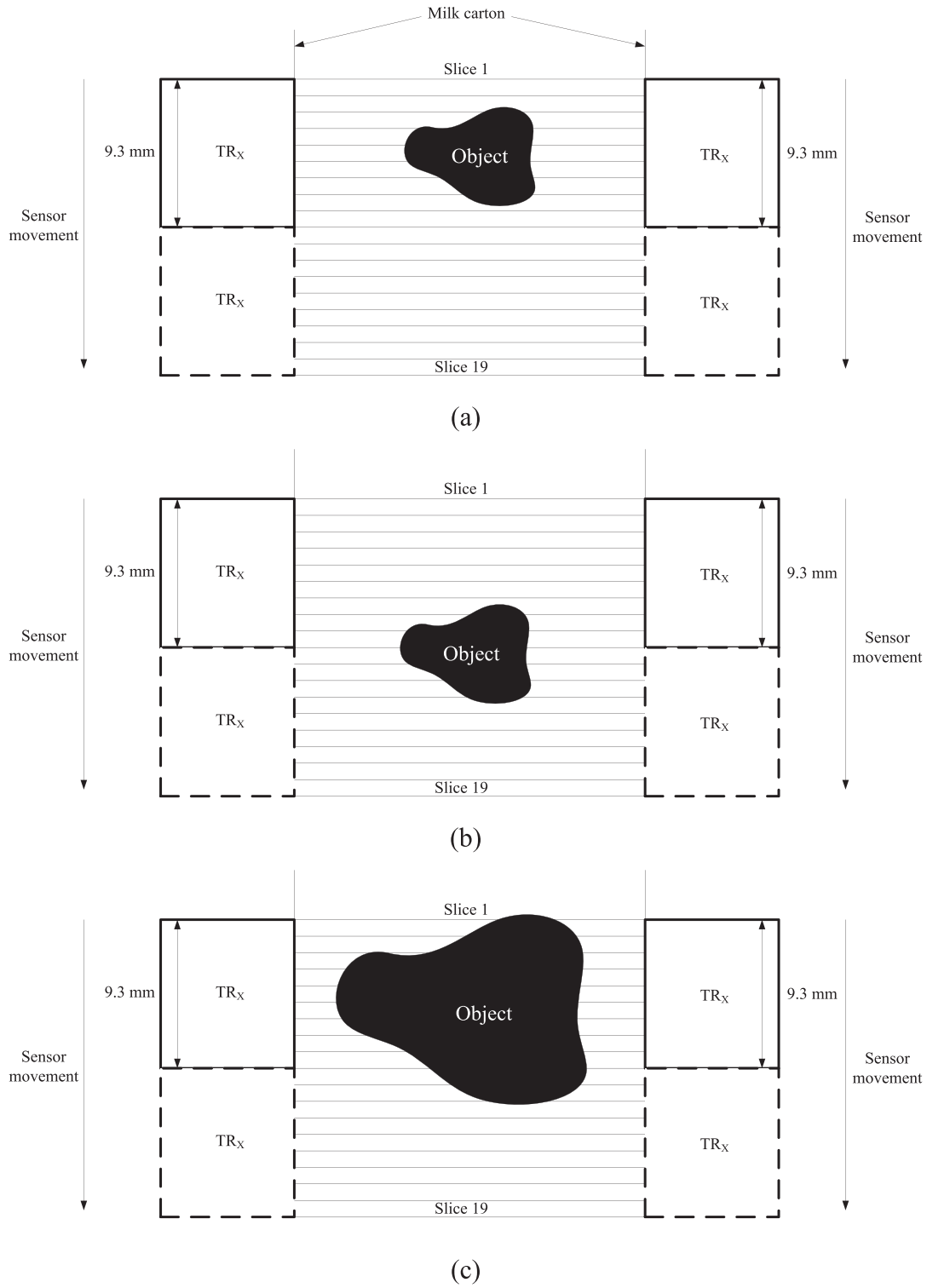


Fig. 12. The illustration of the foreign object position and sensors (a) The object is completely within the projection path for the first movement (b) The object located between two sensors for the first and second movement (c) The object located inside and outside the projection path for the first movement.

mean square error (MSE). The MSE measures the average of the squares of the errors and the difference between the real image and the reconstructed image. MSE is defined as:

$$MSE = \frac{1}{mn} \sum_{i=1}^m \sum_{j=1}^n [A(i, j) - B(i, j)]^2 \quad (5)$$

where, A is the actual image, B is the reconstructed image, m and n are the size of images A and B respectively. Therefore, the PSNR (in dB) can

be formulated as:

$$PSNR = 10 \log_{10} \left(\frac{MAX_A^2}{MSE} \right) = 20 \log_{10} \left(\frac{MAX_A}{\sqrt{MSE}} \right) \quad (6)$$

where MAX_A is the maximum value of pixel in image A . The lower the value of MSE and the higher the PSNR value show that the quality of tomogram image is excellent. PSNR had been applied by Muji [36] and Faramarzi [28]. It works by comparing the “true” pixel values

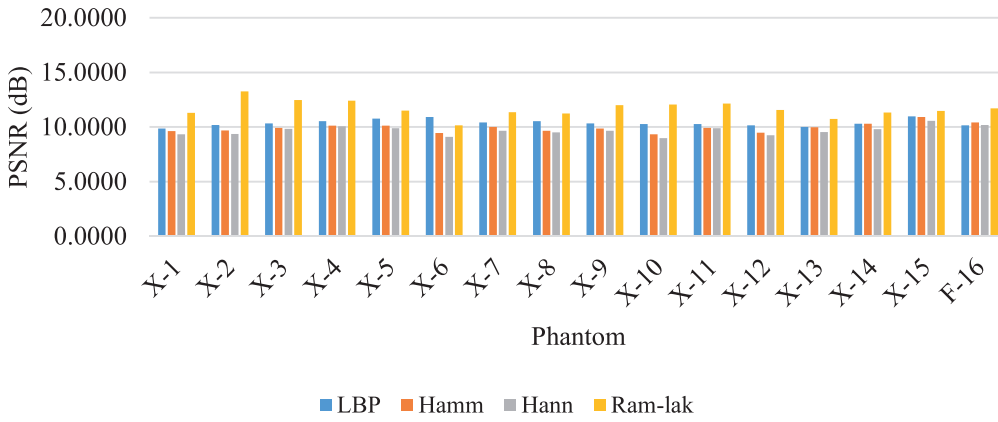


Fig. 13. PSNR graph for group without median filter application.

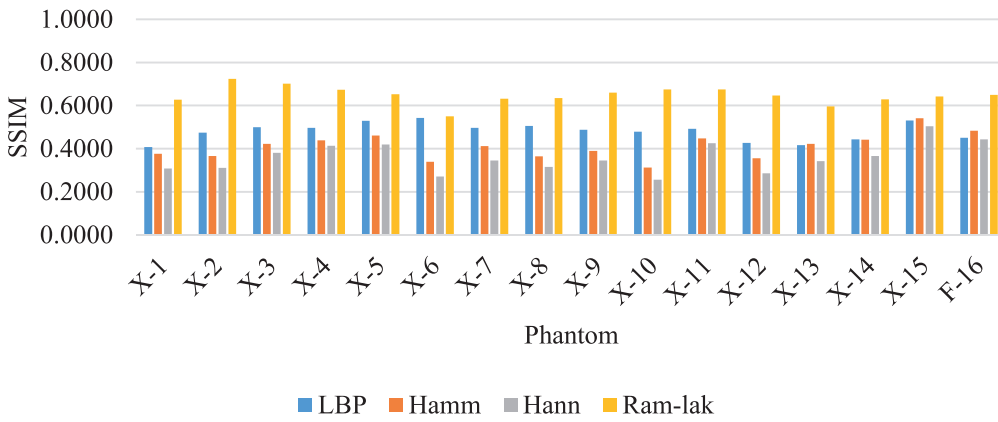


Fig. 14. SSIM graph for group without median filter application.

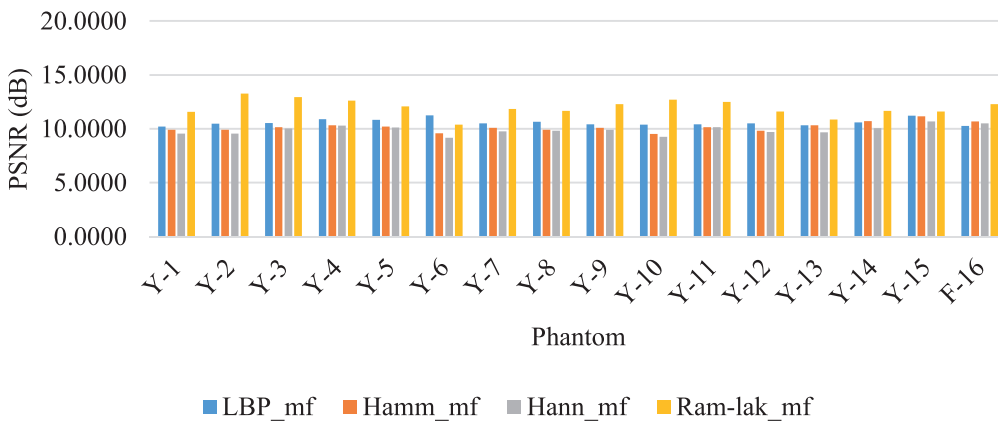


Fig. 15. PSNR graph for group using a median filter.

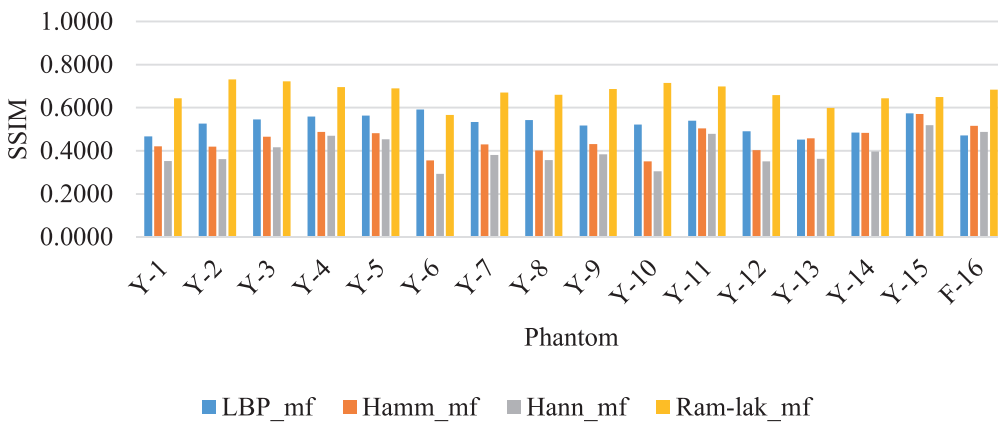


Fig. 16. SSIM graph for group using a median filter.

Table 11
PSNR and SSIM index for group using a median filter.

| Phantom | LBP Mfilter | | CBP-Hamm Mfilter | | CBP-Hann Mfilter | | CBP-Ram-Lak Mfilter | |
|---------|----------------|---------------|------------------|--------|------------------|---------------|---------------------|---------------|
| | PSNR (dB) | SSIM | PSNR (dB) | SSIM | PSNR (dB) | SSIM | PSNR (dB) | SSIM |
| Y-1 | 10.1963 | 0.4662 | 9.9194 | 0.4211 | 9.5652 | 0.3531 | 11.5737 | 0.6439 |
| Y-2 | 10.4834 | 0.5260 | 9.9213 | 0.4190 | 9.5535 | 0.3615 | 13.2765 | 0.7318 |
| Y-3 | 10.5445 | 0.5453 | 10.1522 | 0.4650 | 10.0345 | 0.4167 | 12.9501 | 0.7228 |
| Y-4 | 10.8793 | 0.5589 | 10.3170 | 0.4882 | 10.2942 | 0.4694 | 12.5973 | 0.6959 |
| Y-5 | 10.8374 | 0.5633 | 10.1931 | 0.4811 | 10.1169 | 0.4537 | 12.0728 | 0.6902 |
| Y-6 | 11.2449 | 0.5923 | 9.5718 | 0.3553 | 9.1663 | 0.2937 | 10.3794 | 0.5664 |
| Y-7 | 10.5081 | 0.5344 | 10.0721 | 0.4295 | 9.7592 | 0.3805 | 11.8480 | 0.6698 |
| Y-8 | 10.6624 | 0.5429 | 9.9187 | 0.4012 | 9.8136 | 0.3566 | 11.6641 | 0.6601 |
| Y-9 | 10.4034 | 0.5180 | 10.0982 | 0.4313 | 9.9006 | 0.3842 | 12.2744 | 0.6873 |
| Y-10 | 10.3778 | 0.5220 | 9.5320 | 0.3507 | 9.2563 | 0.3051 | 12.6958 | 0.7156 |
| Y-11 | 10.3996 | 0.5392 | 10.1432 | 0.5041 | 10.1542 | 0.4792 | 12.4899 | 0.6987 |
| Y-12 | 10.4921 | 0.4908 | 9.8072 | 0.4029 | 9.6882 | 0.3506 | 11.5976 | 0.6587 |
| Y-13 | 10.3146 | 0.4513 | 10.3373 | 0.4578 | 9.6738 | 0.3634 | 10.8534 | 0.5997 |
| Y-14 | 10.5912 | 0.4844 | 10.7181 | 0.4838 | 10.0588 | 0.3963 | 11.6588 | 0.6438 |
| Y-15 | 11.2106 | 0.5740 | 11.1457 | 0.5705 | 10.6723 | 0.5182 | 11.5893 | 0.6492 |
| Y-16 | 10.2560 | 0.4711 | 10.6891 | 0.5152 | 10.4954 | 0.4870 | 12.2994 | 0.6839 |
| Average | 10.5876 | 0.5238 | 10.1586 | 0.4485 | 9.8876 | 0.3981 | 11.9887 | 0.6698 |
| SD | 0.3112 | 0.0410 | 0.4219 | 0.0586 | 0.4137 | 0.0663 | 0.7522 | 0.0438 |

*Bold numbers show the highest value of the test phantom.

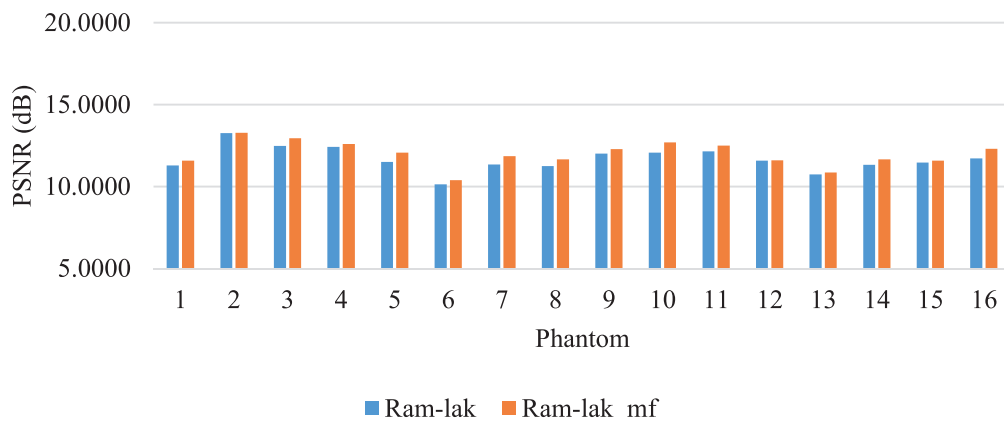


Fig. 17. The PSNR comparison for CBP-Ram-Lak.

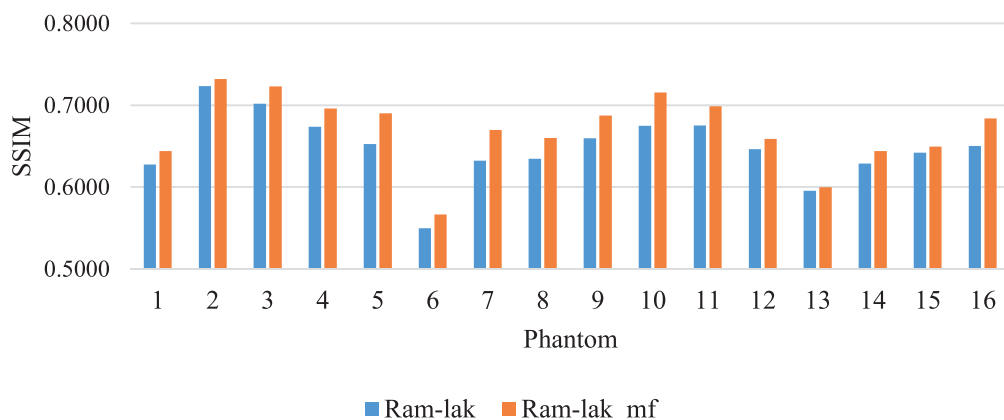


Fig. 18. The SSIM comparison for CBP-Ram-Lak.

of original image to degraded image. The main limitation of this metric is that it relies strictly on numeric comparison and does not actually take into account any level of biological factors of the human vision system [37].

On the other hand, the SSIM index is a method for measuring the similarity between two images. The value of this index is between 0 and 1 and values closer to 1 mean that it has a higher similarity. The SSIM metric is calculated in various windows of an image. The measure

between two windows x and y of common size $N \times N$ is:

$$SSIM(x, y) = \frac{(2\mu_x\mu_y + c_1)(2\sigma_{xy} + c_2)}{(\mu_x^2 + \mu_y^2 + c_1)(\sigma_x^2 + \sigma_y^2 + c_2)} \tag{7}$$

where, μ_x is the average of x , μ_y is the average of y , σ_x^2 is the variance of x , σ_y^2 is the variance of y , σ_{xy} is the covariance of x and y , $c_1 = (k_1L)^2$ and $c_2 = (k_2L)^2$ are two variables which stabilize the division with a weak

Table 12
The process of 2D slice images before reconstructing the pseudo 3D image.

| Phantom | Object and position | CBP-Ram-Lak image | Median filter | Threshold | 8-bit and grayscale |
|---------|---|-------------------|---------------|-----------|---------------------|
| Z-1 | Type: Glass A Position: Middle of the carton (a) 1 st sensors movement (b) 2 nd sensors movement | | | | |
| | | | | | |
| Z-2 | Type: Metal B Position: Bottom and edge of the carton (a) 1 st sensors movement | | | | |
| Z-3 | Type: Wood A Position: Middle of the carton (a) 1 st sensors movement | | | | |
| Z-4 | Type: Wood B and Glass B Position: Middle of the carton (a) 1 st sensors movement | | | | |
| Z-5 | Type: Plastic B and Metal B Position: Middle of the carton (a) 1 st sensors movement | | | | |
| Z-6 | Type: Plastic A and Metal A Position: Middle of the carton (a) 1 st sensors movement (b) 2 nd sensors movement | | | | |
| | | | | | |

denominator [28]. SSIM had been applied by Wang et al [38]., Torras-Rosell et al [39]. as well as Pambrun and Noumeir [40]. SSIM has independent of the luminance and contrast of the local patches [41]. But the limitation is inability to measure highly blurred images [42].

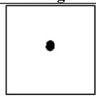

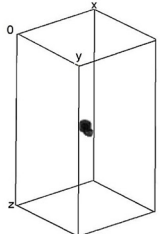
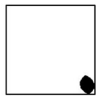
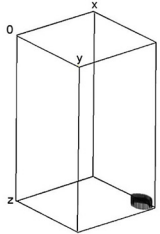
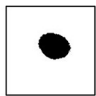
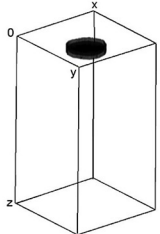

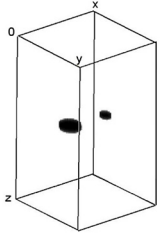
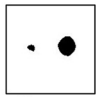
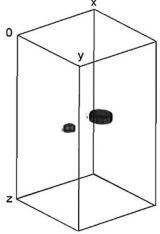

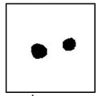
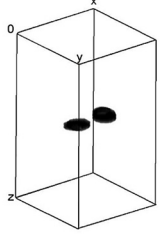
2.7. Pseudo three-dimensional (3D) image reconstruction

The ultrasonic sensor jig is moved from top to bottom of the carton in the z-axis direction to capture the data. The data is useful to reconstruct the 2D cross-sectional images slices. The 2D images are reconstructed using CBP-Ram-Lak since it has less noise and has the sharpest image. Then, the images are merged with the median filter (20 × 20 matrix) and the thresholding technique to reduce the noise. The range of threshold value is from 0.3 to 0.8 for red, blue and green (RGB) colour. The range was selected based on experiment that had been conducted. Each sample may provide the same value. Otherwise, the threshold value need to change by try and error in order to obtain the clear image/adequate. The images are converted into 8-bit and a grayscale colour. Finally, all the images are stacked together using ImageJ software in order to get a 3D image. The stacking of the 2D images is illustrated in Fig. 8. It is assumed that each slice has the thickness of 1 mm, so that the pseudo 3D reconstruction image has a total of 190 slices corresponding to the length of the carton. Fig. 9 shows the summary of the 3D reconstruction process.

The foreign objects were placed in three different positions which is top, middle and bottom of the carton for pseudo 3D image reconstruction. The objects were tied using wire to locate and fixed the positions as shown in Fig. 10. The ultrasonic sensors were moved from the top to the bottom of the carton to obtain the 2D slices images for the whole carton. The carton has height of 190 mm, but the milk is filled only up to 170 mm. Assume that each movement of the sensors will obtain 10 slices of cross-sectional images taking into account of the fact that each sensor has a size of 9.3 mm as illustrated in Fig. 11. Hence, the sensors are moved in 17 steps to evaluate the entire carton. A total of 170 2D slices images are stacked together to create pseudo 3D images from using the ImageJ software.

Fig. 12(a) to (c) show three different cases in which the foreign object could be located when the sensors are moving. The first case is shown in Fig. 12(a) which demonstrated that the sensors could detect the whole object since the whole object is located completely within the projection path. The sensor can detect the object and obtain the 10 slices of images. The second case is illustrated in Fig. 12(b), where the object is located in the middle of the sensor movement. The first and second movement of the sensors might detect the object and could obtain the 20 slices images for this type of case. The last case involves an object which is larger than the sensor as shown in Fig. 12(c). Similar to the second case, this case also might to obtain 20 slices for the first and second movement of the sensors.

Table 13
2D grayscale image and pseudo 3D image reconstruction.

| Phantom | Object and Position | 2D Grayscale Image | 3D Image |
|---------|---|--|--|
| Z-1 | Type: Glass A Position: Middle of the carton |  1 st sensors movement  2 nd sensors movement |  |
| Z-2 | Type: Metal B Position: Bottom and edge of the carton |  1 st sensors movement |  |
| Z-3 | Type: Wood A Position: Top of the carton |  1 st sensors movement |  |
| Z-4 | Type: Wood B and Glass B Position: Middle of the carton |  1 st sensors movement |  |
| Z-5 | Type: Plastic B and Metal B Position: Middle of the carton |  1 st sensors movement |  |
| Z-6 | Type: Plastic A and Metal A Position: Middle of the carton |  1 st sensors movement  2 nd sensors movement |  |

3. Result and discussion

Table 7 shows the types and size of various objects used in the experiment. Each material consists of two different sizes which the range is from 10 to 22 mm.

3.1. 2D image reconstruction

The images of object in category A and B have been reconstructed using LBP, CBP-Hamm, CBP-Hann and CBP-Ram-Lak as shown in Table 8 Table 9 shows the images using a median filter.

The PSNR and SSIM of the reconstructed images are measured and analysed to assess the quality of images. The evaluated results are tabulated as in Tables 10 and 11. Figs. 13 to 16 illustrate the graph patterns for PSNR and SSIM.

Table 8 shows the results of the cross-sectional reconstructed images obtained using LBP, CBP-Hanning, CBP-Hamming, and CBP-Ram-Lak without median filter Table 9. shows the reconstructed images using a median filter which has reduced the noise at the edge of the cartons. As can be seen, all test phantoms could be visualised successfully using CBP-Ram-Lak, while the other algorithms had not provided the sufficient sharp images due to the noise existence. The ramp filter is a compensatory filter as it eliminates the star artefact. This filter has the effect of filtering out low frequencies and passing high frequencies with a linear behaviour. High pass filters have sharpened the edges of the images and enhance the quality of the image.

The PSNR and SSIM assessments for the images are tabulated in Tables 10 and 11, whereas the bar charts of the data are shown in Figs. 13–16. High PSNR values have indicated that the CBP-Ram-Lak image has produced the best tomogram images compared to other algorithms except for the X-6 and Y-6 phantoms. The X-2 phantom has the best PSNR value of 13.2687 for non-median filters and 13.2765 for median filter applications in Y-2 phantom. As for the SSIM parameters, CBP-Ram-Lak filter has revealed that it is the best algorithm for image reconstruction for all sixteen phantoms. Similar to PSNR, SSIM also recorded that X-2 phantom and Y-2 phantom have the best values which are 0.7234 and 0.7318 for categories of non-median filter and median filter applications, respectively.

The images obtained using the median filter is shown in Table 11. The filter has sharpened the image and the noise at the edge of the images have also been reduced especially for CBP-Ram-Lak filters. The comparison of PSNR result for non-median filter and median filter application is shown in Fig. 17. It indicated that all sixteen phantoms have higher PSNR for CBP-Ram-Lak combined with median filter where phantom 2 has obtained the highest value for PSNR = 13.2765, whereas CBP-Ram-Lak without median filter has PSNR = 13.2687. The comparison for SSIM values is demonstrated in Fig. 18 and the data shows that the SSIM values using median filter also have the best results for all sixteen test phantoms. The median filter result for phantom 2 shows the highest value of SSIM with 0.7318, a bit higher than obtained by CBP-Ram-Lak without median filter which is 0.7234.

3.2. Pseudo 3D image reconstruction

This section showed the pseudo 3D image reconstruction for the foreign object that exist inside the milk carton. The foreign objects were placed in three different positions which is top, middle and bottom of the carton for pseudo 3D image reconstruction. The ultrasonic sensor jig is moved from top to bottom of the carton in the z-axis direction to capture the data. The data is used to reconstruct the 2D cross-sectional images slices. The 2D images are reconstructed using CBP-Ram-Lak since it has less noise and has the sharpest image. The 2D slice images and the 3D images for the tested object is shown in Table 12 and Table 13, respectively.

As discussed before, there are three different cases in which the foreign object could be located when the sensors are moving as illustrated

in Fig. 12. These cases have resulted the number of slice image for each sensor movement. In Table 12, phantom Z-1 (glass A) and phantom Z-6 (plastic A and metal A) has been detected with two steps of the sensors movement. It may due to the objects have a larger size than the sensor. The other possibility is the objects are located between the sensors movement. The slices obtained for each of these two phantoms are 20 slices out of 170 total slices for the whole carton. The other phantoms (Z-2, Z-3, Z-4 and Z-5) can be detected with a single step of sensors movement only. It might be the objects may be located completely within the projection path and the size is not larger than the sensors. The total slices obtained for each phantom are 10 slices out of 170 total slices for whole carton. All 2D slices images are stacked together to reconstruct the pseudo 3D image as shown in Table 13. The location of the object inside the carton filled by milk is visualised clearly either it is located in top, middle or bottom of the carton. The ultrasonic tomography system has able to detect and reconstruct the presence of foreign object in milk products. In addition, the exact location of the object can be visualised clearly from various view angles using pseudo 3D image reconstruction.

4. Conclusions

An ultrasonic tomography method for identifying external substances particularly solid item in milk product has been effectively evolved. The LBP and CBP algorithms with Hanning, Hamming and Ram-Lak filters were implemented to reconstruct two-dimensional cross-sectional images of the milk and the foreign objects. The results show that the measurement system is capable of reconstructing the object. A microcontroller unit (dsPIC30F6014) was implemented in the system to integrate the hardware and the software systems. The microcontroller also controls the digital signal and operates as a data acquisition system. Based on the obtained data, the integration system has successfully reconstructed the tomogram image. High-density and low-density foreign objects have been placed inside a milk carton for evaluation. The objects consist of metal, glass, wood and plastic and each type have different sizes. The objects are successfully reconstructed and visualized by the measurement system. Median filters with 20×20 matrix had been implemented in order to minimize the noise. The analysis based on PSNR and SSIM evaluation demonstrated that CBP-Ram-Lak filters with median filter applications have produced the best performance and provide sharper images compared to other types of algorithms. Pseudo 3D images also have been reconstructed based on stacking the 2D cross-sectional images using ImageJ software. Therefore, the exact location of the foreign object could be obtained.

Acknowledgements

The authors would like to acknowledge the assistance of the Ministry of Higher Education Malaysia under the MyBrain15 program and Universiti Teknologi Malaysia for providing the research grants 15H85 and 4J255 which enabled this research to be carried out.

References

- [1] M.S. Park, H.N. Kim, G.J. Bahk, The analysis of food safety incidents in South Korea, 1998–2016, *Food Control* 81 (2017) 196–199.
- [2] I. Djekic, D. Jankovic, A. Rajkovic, Analysis of foreign bodies present in European food using data from rapid alert system for food and feed (RASFF), *Food Control* 79 (2017) 143–149.
- [3] E.C. Mattos, V.S.M.G. Daros, R. Dal Col, A.L. Nascimento, Occurrence of foreign matter in food: applied identification method-association of official agricultural chemists (AOAC) and food and drug administration (FDA), *Int. J. Biol. Biomol. Agric. Food Biotechnol. Eng.* 10 (2016) 101–105.
- [4] R.S. Aguiar, E.A. Esmerino, R.S. Rocha, T.C. Pimentel, V.O. Alvarenga, M.Q. Freitas, M.C. Silva, A.S. Sant'Ana, A.C.O. Silva, A.G. Cruz, Physical hazards in dairy products: incidence in a consumer complaint website in Brazil, *Food Control* 86 (2018) 66–70.
- [5] BBC News, "What's that in my milk?", (2009). https://www.bbc.co.uk/guernsey/content/articles/2009/06/23/found_in_milk_feature.shtml (accessed August 20, 2018).
- [6] CBC News, Milk products recalled in Ont. over glass hazard, (2011). <https://ottawa.ctvnews.ca/milk-products-recalled-over-glass-fragments-1.628622> (accessed August 20, 2018).

- [7] BBC News, Man claims “pin-like” objects found in Strathroy dairy milk, (2011). <https://www.bbc.com/news/uk-northern-ireland-15104040#:~:text=An%20omagh%20dairy%20is%20under,the%20Lidl%20store%20in%20Strabane> (accessed August 20, 2018).
- [8] Australia Food News, Milk recalled after foreign body “similar in appearance to hair” identified in product, (2012). <https://www.ausfoodnews.com.au/2012/04/19/milk-recalled-after-foreign-body-similar-in-appearance-to-hair-identified-in-product.html> (accessed August 20, 2018).
- [9] CBC News, Slimy object found in St. John’s woman’s almond milk was just mould, (2015). <https://www.cbc.ca/news/canada/newfoundland-labrador/slimy-object-found-in-st-john-s-woman-s-almond-milk-was-just-mould-1.3017813#:~:text=25-,A%20st.,sort%20of%20snake%20or%20worm> (accessed August 20, 2018).
- [10] Komonews, Couple: screw found in son’s sippy cup came from milk carton, (2015). <https://komonews.com/news/local/couple-screw-found-in-sons-sippy-cup-came-from-milk-carton> (accessed August 20, 2018).
- [11] Sfgate, Clover recalls milk products over small pieces of plastic, (2015). <https://www.sfgate.com/bayarea/article/Clover-recalls-milk-products-over-small-pieces-of-6393852.php> (accessed August 20, 2018).
- [12] Hong Kong Free Press, Internet united in disgust after ‘alien’ object found in rice milk carton, (2016). <https://hongkongfp.com/2016/03/26/internet-united-in-disgust-after-alien-object-found-in-rice-milk-carton/> (accessed August 20, 2018).
- [13] Channel News Asia, Woman finds unidentified object in toddler’s Marigold milk, (2016). <https://www.channelnewsasia.com/news/singapore/woman-finds-unidentified-object-in-toddler-s-marigold-milk-7770948> (accessed August 20, 2018).
- [14] Food Standard Australia New Zealand, Lactose free whole milk powder, (2018). <http://www.foodstandards.gov.au/industry/foodrecalls/recalls/Pages/Lactose-Free-Whole-Milk-Powder.aspx> (accessed August 20, 2018).
- [15] R.P. Haff, N. Toyofuku, X-ray detection of defects and contaminants in the food industry, *Sens. Instrum. Food Qual. Saf.* 2 (2008) 262–273.
- [16] P. Pallav, G.G. Diamond, D.A. Hutchins, R.J. Green, T.H. Gan, A near-infrared (NIR) technique for imaging food materials, *J. Food Sci.* 74 (2009) 23–33.
- [17] S.N. Jha, K. Narsaiah, A.L. Basediya, R. Sharma, P. Jaiswal, R. Kumar, R. Bhardwaj, Measurement techniques and application of electrical properties for nondestructive quality evaluation of foods – a review, *J. Food Sci. Technol.* 48 (2011) 387–411.
- [18] L. Senni, P. Burrascano, M. Ricci, Multispectral laser imaging for advanced food analysis, *Infrared Phys. Technol.* 77 (2016) 179–192.
- [19] Z. Xiong, D.W. Sun, X.A. Zeng, A. Xie, Recent developments of hyperspectral imaging systems and their applications in detecting quality attributes of red meats: a review, *J. Food Eng.* 132 (2014) 1–13.
- [20] M.T.M. Khairi, S. Ibrahim, M.A.M. Yunus, M. Faramarzi, Ultrasonic tomography for detecting foreign objects in refrigerated milk cartons, *Int. J. Dairy Technol.* 71 (2018) 1–7.
- [21] M.T.M. Khairi, S. Ibrahim, M.A.M. Yunus, M. Faramarzi, G.P. Sean, J. Puspanathan, A. Abid, Ultrasound computed tomography for material inspection : principles, design and applications, *Measurement* 146 (2019) 490–523.
- [22] S. Ibrahim, M.A.M. Md Yunus, M.T.M. Khairi, M. Faramarzi, A review on ultrasonic process tomography system, *J. Teknol.* 70 (2014) 1–5.
- [23] Warsito, M. Ohkawa, N. Kawata, S. Uchida, Cross-sectional distributions of gas and solid holdups in slurry bubble column investigated by ultrasonic computed tomography, *Chem. Eng. Sci.* 54 (1999) 4711–4728.
- [24] M.C. Edwards, *Detecting Foreign Bodies in Food*, Woodhead Publishing Limited, Cambridge, England, 2004.
- [25] M.T.M. Khairi, S. Ibrahim, M.A.M. Yunus, M. Faramarzi, Noninvasive techniques for detection of foreign bodies in food: a review, *J. Food Process Eng.* 41 (2018) 1–20.
- [26] R.A. Rahim, M.H.F. Rahiman, C.L. Goh, S.Z.M. Muji, H.A. Rahim, Y.M. Yunus, Modeling orthogonal and rectilinear mixed-modality projection of optical tomography for solid-particles concentration measurement, *Sens. Actuators A Phys.* 161 (2010) 53–61.
- [27] M.H.F. Rahiman, R.A. Rahim, H.A. Rahim, Z. Zakaria, M.J. Puspanathan, A study on forward and inverse problems for an ultrasonic tomography, *J. Teknol.* 70 (2014) 113–117.
- [28] M. Faramarzi, *Image Reconstruction Technique for Ultrasonic Transmission Tomography*, Universiti Teknologi Malaysia, 2016 PhD Thesis.
- [29] J. Puspanathan, *Dual Modality Tomography for Multiphase Flow Imaging Using Electrical Capacitance and Ultrasonic Sensors*, Universiti Teknologi Malaysia, 2016 PhD Thesis.
- [30] R. Cierniak, An analytical iterative statistical algorithm for image reconstruction from projections, *Int. J. Appl. Math. Comput. Sci.* 24 (2014) 7–17.
- [31] S. Rit, D. Sarrut, L. Desbat, Comparison of analytic and algebraic methods for motion-compensated cone-beam CT reconstruction of the thorax, *IEEE Trans. Med. Imaging* 28 (2009) 1513–1525.
- [32] P.P. Bruyant, Analytic and iterative reconstruction algorithms in SPECT, *J. Nucl. Med.* 43 (2002) 1343–1358.
- [33] G.L. Zeng, Noise handling, in: *Medical Image Reconstruction: A Conceptual Tutorial*, 1st ed., Springer, Berlin, Germany, 2009, pp. 125–170.
- [34] C.J. Du, D.W. Sun, Recent developments in the applications of image processing techniques for food quality evaluation, *Trends Food Sci. Technol.* 15 (2004) 230–249.
- [35] B.B. Parfenenkov, M.A. Panachev, Comparison of some image quality approaches. *CEUR Workshop Proceedings*, 2014, 1197, pp. 48–53.
- [36] S.Z. Mohd Muji, *Optical Tomography for Solid Gas Measurement Using Mixed Projection*, Universiti Teknologi Malaysia, Skudai, 2012 PhD Thesis.
- [37] K. Seshadrinathan, T.N. Pappas, R.J. Safranek, J. Chen, Z. Wang, H.R. Sheikh, A.C. Bovik, *Image Quality Assessment*, 2nd ed., Elsevier, USA, 2009.
- [38] Z. Wang, A.C. Bovik, H.R. Sheikh, E.P. Simoncelli, Image quality assessment: from error visibility to structural similarity, *IEEE Trans. Image Process.* 13 (2004) 600–612.
- [39] A. Torras-Rosell, O. Lylloff, S. Barrera-figueroa, F. Jacobsen, Reconstruction methods for sound visualization based on acousto-optic tomography, in: *Proceedings of the INTER-NOISE*, Innsbruck, Austria, 2013, pp. 1–9.
- [40] J.F. Pambrun, R. Noumeir, Limitations of the SSIM quality metric in the context of diagnostic imaging, in: *Proceedings of the International Conference on Image Processing (ICIP)*, 2015, pp. 1–5.
- [41] G.P. Renieblas, E.G. del Castillo, N. Gómez-Leon, A.M. González, A.T. Nogués, Structural similarity index family for image quality assessment in radiological images, *J. Med. Imaging.* 4 (2017) 035501.
- [42] D. Sadykova, A.P. James, Quality assessment metrics for edge detection and edge-aware filtering: a tutorial review, in: *Proceedings of the International Conference on Advances in Computing, Communications and Informatics (ICACCI)*, 2017, pp. 2366–2369.